Available online at www.sciencedirect.com
SCIENCE DIRECT®
Cement & Concrete Composites 27 (2005) 823–833
Cement & Concrete Composites
www.elsevier.com/locate/cemconcomp

Morphological operations, planar mathematical formulations, and stereological interpretations for automated image analysis of concrete microstructure

Parviz Soroushian *, Mohamed Elzafraney

Civil and Environmental Engineering Department, Michigan State University, 3546 Engineering Building, East Lansing, Michigan 48824-1226, USA

Received 2 September 2003; accepted 22 July 2004

Abstract

Different morphological routines were tailored towards processing and analysis of concrete microstructural images captured by environmental scanning electron and fluorescent microscopy. These routines transform concrete micrographs form gray scale to binary scale, and remove most of the noise without significantly disturbing the features of interest (microcracks and air voids). Formulations are developed for quantification of key features of concrete microcracks and voids systems in plane. Stereological relationships are presented for development of quantitative information on (3-D) structure of concrete microcracks and voids systems in terms of (2-D) data generated from perpendicular sections. Image processing routines, in-plane formulations, and in-space interpretations were addressed to be transformed into algorithms to be built in newly developed computer software for microstructural analysis of concrete.

Keywords: Microcracks; Voids; Concrete; Image processing; Image analysis; Stereology; Measurements; Quantification

1. Introduction

Qualitative microstructural investigation of concrete is broadly used towards assessment of concrete composition [1–6], investigate the effect of different loading types on concrete failure process and its mechanical properties [7–10], and study the influence of various environmental and durability conditions on concrete performance [11–14]. Although qualitative microstructural studies provide insight into concrete microstructure, quantitative information would be needed for such purposes as validation of theories of concrete failure and statistical analysis of damage and failure processes. Latest developed computer-based image analysis techniques [15] provide strong tools which can be adapted towards quantitative microstructural investigation of concrete. These techniques together with stereological techniques can be used to provide quantitative information of such structural phenomenal as spatial growth of microcracks in concrete under damaging effects.

Image processing, image analysis, and stereological aspects are employed in the proposed approach to yield quantitative information on the three-dimensional structure of microcracks and voids systems in concrete. Image processing can manipulate images and rearranges them with the intention of making them more useful, but cannot reduce (or increase) the amount of data present in the original image [16]. The ultimate goal of image processing is to extract feature topology from digitized images of the material, yielding quantitative information on features and phases of interest [16]. In order to

* Corresponding author. Tel./fax: +1 517 355 2216.
E-mail address: soroushi@egr.msu.edu (P. Soroushian).

0958-9465/$ - see front matter © 2005 Elsevier Ltd. All rights reserved.
doi:10.1016/j.cemconcomp.2004.07.008

Nomenclature

Notations

A_{AC1}	crack area fraction on the first (horizontal) section
A_{AC2}	crack area fraction on the second (vertical) section
A_{Ag}	aggregate area fraction
A_{iC}	area of each individual crack
A_{icm}	mean of the area of each individual crack in the section of interest
A_{ig}	area of each individual aggregate particle
A_{iv}	area of each individual void
A_{sg}	aggregate particles aspect ratio
$(A_{Sf})_{av}$	average value of fibers aspect ratio in the whole section of interest
d_{if}	diameter of each individual fiber
d_v	diameter of individual void in the section of interest
d_{vn}	diameter of "n" voids in the section of interest
h_{if}	height of each individual fiber
h_{mf}	average height of fibers in section of interest
L	dimension of the section of interest
L_{AC1}	crack length per unit area of the first (horizontal) section (perpendicular to the direction of loading)
L_{AC2}	crack length per unit arc of the second (vertical) section [Perpendicular to the first (horizontal) section)]
L_g	length of any individual aggregate particle in the section of interest
L_{gn}	length of "n" aggregate particles in the section of interest
L_{iC}	length of each individual crack
L_{ig}	length of each individual aggregate particle
L_{iv}	length (longest diameter) of each individual void
N_{Af}	number of fibers per unit area
N_{Ag}	number of aggregate particles per unit area of section of interest
N_{AV}	number of voids per unit volume
n_g	number of aggregate particles in the section of interest
N_{iv}	total number of voids in the whole section
N_{LC}	number of cracks through length (L)
N_{SC}	total number of cracks in the section of interest
n_v	number of voids in the section of interest
P_{iC}	perimeter of each individual crack
P_{iv}	perimeter of each individual void
$(PL)_{iav}$	average (PL) value for each individual aggregate
$(PL)i\perp$ or $(PL)i\parallel$	number of point intersections per unit length of superimposed array of equally spaced parallel test lines oriented in a predetermined direction for each individual aggregate particle. Subscripts "$\perp$" and "$\parallel$" refer to test lines running perpendicular and parallel to the preferred orientation of aggregates
$(PL)t\perp$ or $(PL)t\parallel$	number of point intersections per unit length of superimposed array of equally spaced parallel test lines oriented in a predetermined direction. Subscripts "$\perp$" and "$\parallel$" refer to test lines running perpendicular and parallel to the preferred orientation of cracks. Subscript "t" refers to the total point intersections in a certain direction
$(PL)ts\perp$ or $(PL)ts\parallel$	number of point intersections per unit length of superimposed array of equally spaced parallel test lines oriented in a predetermined direction. Subscripts "$\perp$" and "$\parallel$" refer to test lines running perpendicular and parallel to the preferred orientation of cracks. Subscript "t" refers to the total point intersections in a certain direction. Subscript "s" refers to the point intersections in space
T_{CP1}	crack tortuosity in plane in the first section (perpendicular to direction of loading)
T_{CP2}	crack tortuosity in plane in the second section (perpendicular to the first section)
V_{Vf}	fibers volume fraction
W_{iC}	width of each individual crack
W_{ig}	width of each individual aggregate particle
W_{vc}	width (shortest diameter) of each individual void
λ_{CP1}	spacing in plane through length (L)
λ_{cpx}	spacing in X-direction
λ_{cpy}	spacing in Y-direction
Γ_g	width/length ratio of any individual aggregate particle in the section of interest
Γ_{gn}	width/length ratio of "n" aggregate particle in the section of interest

achieve this objective, a host of image processing and analysis functions have been developed and adapted to identify and then analyze features of interest. The key step in image processing involves separation of features of interest from background. This step typically involves a large number of operations and iterations; hence, selection of appropriate operations and a reasonable number of iterations can help enhance the efficiency of segmentation.

Image analysis is broadly defined as extraction of useful numerical data from an image [16]. Image analysis is generally implemented after image processing steps. Box

counting method is one of the oldest means of determining the fractal dimension of the crack structure [7]. Another approach to image analysis of cracks involves mapping the cracks and manually measuring the length and area of cracks [17]. Image analysis is used to quantify different compounds of concrete, and to assess the characteristics of such components [18]. Finite element and finite difference techniques have been recently incorporated into image analysis schemes in order to determine the properties and assess the distribution of strains within construction materials [19].

Stereology can be defined as a body of mathematical methods which relate three-dimensional parameters defining the structure to two-dimensional measurements obtainable on sections of the structure [20]. Stereological principles can be used to quantify many spatial attributes of oriented features (such as the degree of anisotropy, surface area of oriented cracks per unit volume, and void size distribution) in terms of measurements conducted on perpendicular cross sections.

Different image processing strategies were developed in the current study for application to (fluorescent or environmental scanning electron) microscopic images with the purpose of transforming captured concrete images from gray scale into binary scale images; enhancing the contrast between the features of interest (microcracks and voids) and the body of concrete, and removing noise (speckle) from images to facilitate accurate quantitative measurements of the features of interest. Various strategies were evaluated in order to identify the most successful ones for application to concrete microscopic images. Visilog 5.3® image processing software was used to implement different strategies. Stereological formulations were also adapted to derive quantitative information on spatial attributes of microcrack and void system based on measurements performed on perpendicular cross sections.

2. Morphological operations

The first step in image processing is segmentation (threshold function), which allows distinction of pixels belonging to the feature of interest. After segmentation, neighborhood operations can be employed to refine the form of objects. Such operators, which relate pixels in a small neighborhood, are versatile and powerful tools which combine pixels of binary images with logical operations of Boolean algebra. Five operations were found to be useful in application to concrete microscopic images; these operations cause dilation or erosion of objects. Some morphological operations such as skeletonization and pruning are ignored due to their ability to create thin lines rather than a set of thick (real dimensions) microcracks which may affect area fraction, perimeter and width of microcracks measurements. The selected image processing operations in addition to segmentation, are dilation, erosion, opening, closing, and hole-fill. Dilation has different effects, including filling of small holes or cracks and smoothing of contour lines. Erosion causes disappearance of objects smaller than a mask governing the effect of this operation. Erosion provides the opportunity to eliminate noise but it has the disadvantage that all the remaining objects shrink in size. In order to overcome this problem, erosion and dilation operations may be used together. This largely recovers the original feature size while producing a smooth shape. The sequence of erosion followed by dilation is called an opening. The initial erosion removes small features which may represent noise in concrete micrographs, and also sharp protuberances from the feature outline. The subsequent dilation does not restore the small features (noise), which have permanently disappeared, but it does fill in any small indentations in the outlines. In contrast to erosion, dilation enlarges objects and closes small holes and cracks. General enlargement of the object by the size of mask can be reversed by follow-up erosion. This combination of operations is called closing operation. Dilation operation can fill very small holes in features of interest. If the feature has a large hole within it which does not provide any physical meaning, dilation operation can not regain the missing part at low number of iterations. Increasing the number of dilation iterations to recover the missing hole can damage the whole image by swelling the size of other features. Application of the hole-fill function is essential in this case. The hole-fill function recovers the missing holes within any feature (microcrack or void) without any change to its size. Application of the hole-fill function to microcracks or voids that do not have any holes does not produce any harmful effect on them or the rest of features in the image. Between auto-threshold and hole-fill functions, there are many scenarios can be proposed to achieve the goal of enhancing the features of interest (microcracks and voids); alternative scenarios combined in this work are shown in Fig. 1.

Concrete specimens were prepared by impregnation with Wood's metal for environmental scanning electron microscopy (ESEM) and with ink followed by epoxy for fluorescent microscope. Concrete micrographs were captured using either ESEM or fluorescent microscope, and the alternative image processing scenarios were applied to those images. The effect of applying the alternative scenarios on fluorescent and ESEM micrographs is shown in Figs. 2 and 3, respectively. Applying those scenarios on numerous images showed the best results were generally obtained when Scenario #1 and #7 were implemented. Scenario #1 may be useful when images contain a noticeable number of noise where application of the opening operation first followed by the closing operation probably restore the image after removal of noise. Images containing missing parts of features of

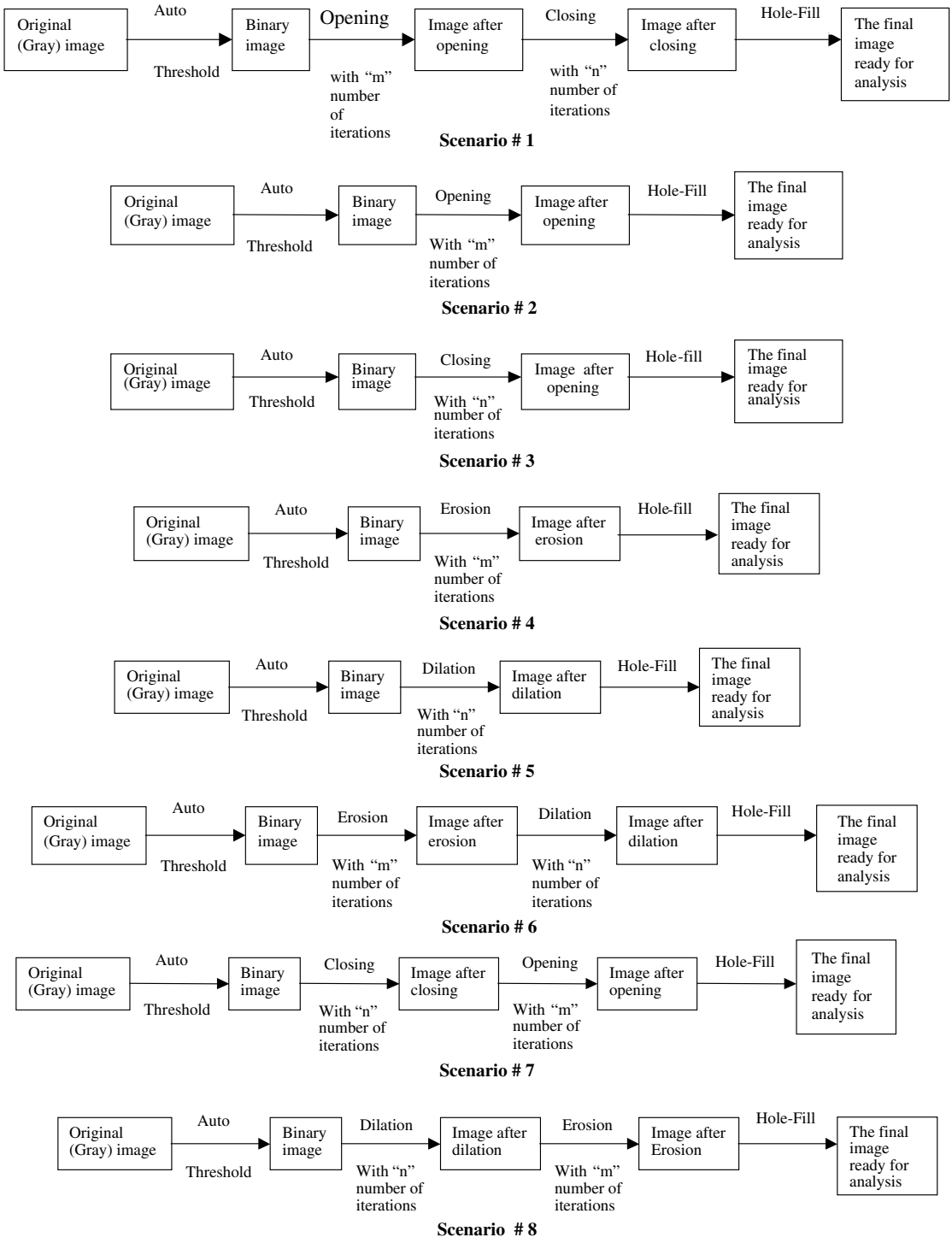

Fig. 1. Proposed image processing scenarios.

interest (microcracks and voids) can benefit from Scenario #7 since the closing operation, when applied first, helps recover some missing parts of the features of interest while preventing further losses in original feature caused by the opening operation. The quality of the original image decide the level of change brought about by any of these scenarios. For example, the generally better quality of environmental scanning electron micrographs, when compared with fluorescent micrographs, implies that ESEM images are less sensitive to the selection of particular image processing scenarios. It should be noted that scanning electron and fluorescent microscopy use specimens impregnated with Wood's metal and fluorescent epoxy, respectively, which could

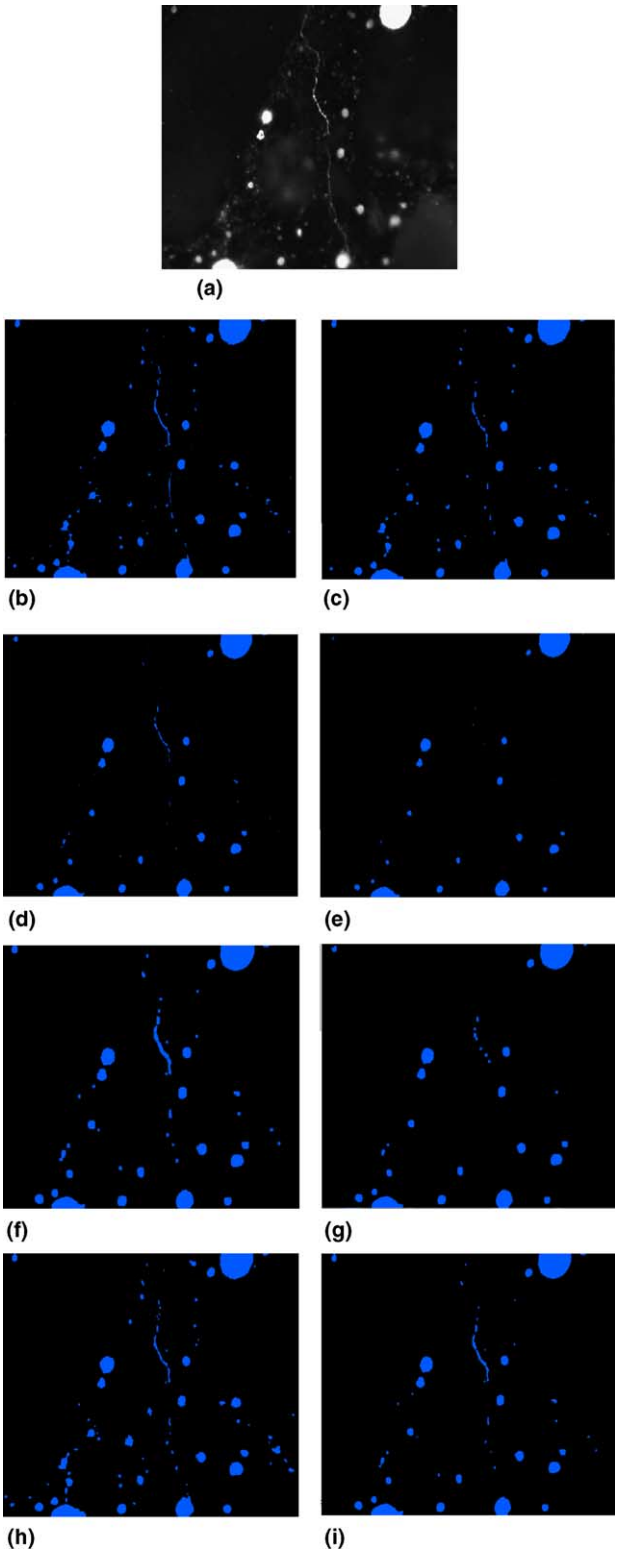

Fig. 2. Effect of applying different image processing scenarios on fluorescent gray scale concrete micrograph at magnification 125×: (a) original gray image, (b) final image (scenario #1), (c) final image (scenario #2), (d) final image (scenario #3), (e) final image (scenario #4), (f) final image (scenario #5), (g) final image (scenario #6), (h) final image (scenario #7) and (i) final image (scenario #8).

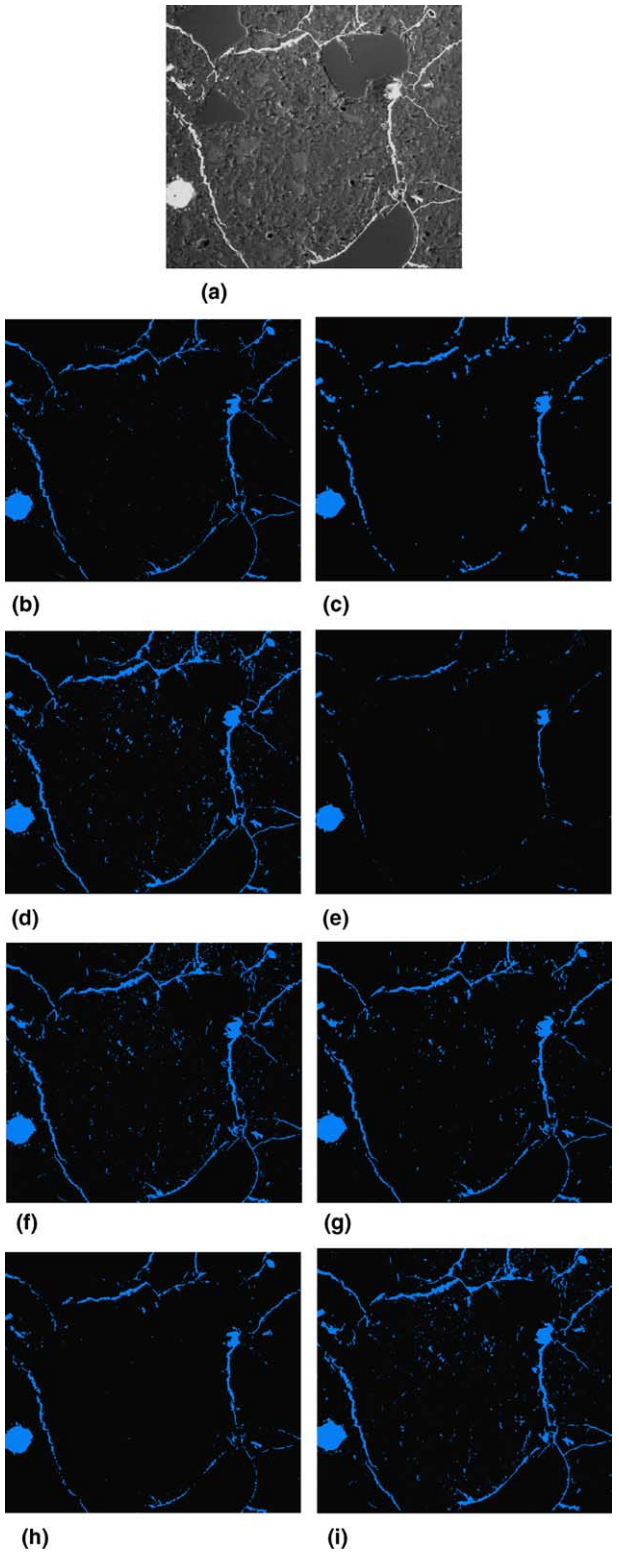

Fig. 3. Effect of applying different image processing scenarios on ESEM gray scale concrete micrograph at magnification 250×: (a) original gray image, (b) final image (scenario #1), (c) final image (scenario #2), (d) final image (scenario #3), (e) final image (scenario #4), (f) final image (scenario #5), (g) final image (scenario #6), (h) final image (scenario #7) and (i) final image (scenario #8).

differ in terms of the thoroughness of impregnation into concrete microcracks and pores. In order to determine the optimum number of iterations in different image processing operations, concrete microscopic images were processed with each scenario using different number of iterations (ranging from 1 to 10). The results suggested that a low number of iterations of the opening function may not efficiently remove the noise from images; a high number of iterations of the opening operation, on the other hand removes parts (pixels) of the feature of interest. In the case of closing operations, a low number of iterations may not effectively restore missing parts of interest, while a high number of iterations could cause noticeably swelling of features, yielding misleading measurements. It was also noticed that using fixed number of closing and opening iterations may not be universally applicable to different image conditions; hence, a range was suggested for the number of iterations for different scenarios. These ranges were (0–2) for opening operation, and (0–3) for closing operation. The optimum number of iterations for certain image condition depends on the amount of noise and the size of noise relative to the size of the features of interest.

3. Mathematical models, in plane (2-D) measurements

3.1. Cracks

3.1.1. Length per unit area (L_{AC})

Crack length per unit area is expresses "crack density" [21] in concrete specimens and provides an indication about crack characteristics in concrete. The crack length per unit area (are of the section of interest) can be expressed as follows:

$$L_{\mathrm{AC}} = \frac{L_{\mathrm{iC}}}{\mathrm{Area}} \tag{1}$$

3.1.2. Perimeter per unit area (P_{AC})

Perimeter tends to be more than twice the length due to the tortuosity and branching effects which increase perimeter but length. Crack Perimeter per unit area can be expressed as follows:

$$P_{\mathrm{AC}} = \frac{P_{\mathrm{iC}}}{\mathrm{Area}} \tag{2}$$

3.1.3. Area fraction (A_{AC})

Cracks Area fraction is considered one of the most important parameters to characterize damage in concrete since increasing crack area fraction in concrete gives an indication that the concrete has high degree of damage. Crack area fraction can be expressed as follows:

$$A_{\mathrm{AC}} = \frac{A_{\mathrm{iC}}}{\mathrm{Area}} \tag{3}$$

3.1.4. Width in plane (W_{CP})

Width is actually defined as breadth, which deviates from actual width for branched and tortuous cracks. Crack width per unit area can be expressed as follows:

$$W_{\mathrm{CP}} = \frac{W_{\mathrm{iC}}}{\mathrm{Area}} \tag{4}$$

Throughout the research an empirical equation was developed to provide crack width measurement. The proposed equation is as follows:

$$W_{\mathrm{CP}} = \frac{3.5 \times A_{\mathrm{iC}}}{\pi \times L_{\mathrm{iC}}} \tag{5}$$

In order to validate the applicability of the proposed equation, 100 different cracks vary in its shape and size were captured at different magnification factors and measured. The actual width of each individual crack was measured manually using Visilog 5.3® and the proposed equation was also applied for the purpose of comparison. The error as a percentage in the calculations of crack width by the proposed equation is shown in Table 1 and the comparison between calculated and measured crack width is shown in Fig. 4.

Table 1
Error in calculated crack width

	Measured crack width	Calculated crack width	Error in calculated crack width (%)
Minimum (pixels)	6.83	5.10	10.2
Maximum (pixels)	262.3	235.5	41.3
Average (pixels)	47.4	36.7	22.9
Standard deviation	50.0	44.5	13.3

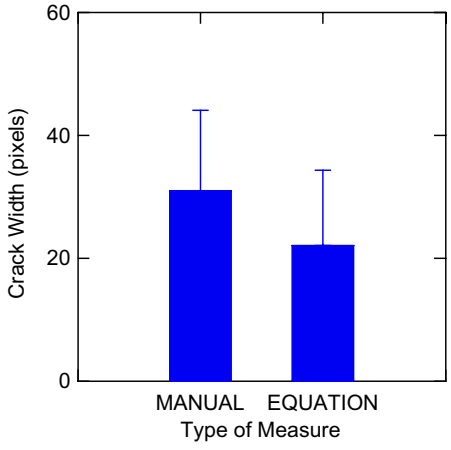

Fig. 4. Comparison between measured and calculated crack width.

3.1.5. Spacing in plane (λ_{CP})

In the simplified model of Fig. 5, it is assumed that each crack can be represented by circle has the same area and positioned in the center of gravity of the crack. It is also assumed that cracks are uniformly and equally distributed in plane (2-D). The crack spacing expression can be derived as follows:

$$\lambda_{\mathrm{CP1}} = \frac{L}{N_{\mathrm{LC}}} \tag{6}$$

The number of cracks along length L can be expressed as follows:

$$N_{\mathrm{LC}} = \sqrt{N_{\mathrm{SC}}} \tag{7}$$

The total number of cracks in the section of interest is

$$N_{\mathrm{SC}} = \frac{\sum A_{\mathrm{iC}}}{A_{\mathrm{icm}}} \tag{8}$$

By substitution of Eqs. (7) and (8) in Eq. (6), the following expression can be obtained:

$$\lambda_{\mathrm{CP1}} = \frac{L}{\sqrt{\sum A_{\mathrm{iC}}/A_{\mathrm{icm}}}} \tag{9}$$

For the purpose of normalization (spacing per unit length), length (L) can be replaced by length per unit area, and the area of cracks can be replaced by area fraction. The crack spacing in plane thus can be expressed as follows:

$$\lambda_{\mathrm{CP}} = \sqrt{\frac{A_{\mathrm{icm}}}{\sum A_{\mathrm{AC}}}} \tag{10}$$

The diagonal spacing can be obtained by using the following expression:

$$\lambda_{\mathrm{CP\,diagonal}} = \sqrt{(\lambda_{\mathrm{cp}x})^2 + (\lambda_{\mathrm{cp}y})^2} \tag{11}$$

Eqs. (10) and (11) yield the following expression for diagonal spacing:

$$\lambda_{\mathrm{Pc\,diagonal}} = \sqrt{2}\sqrt{\frac{A_{\mathrm{icm}}}{\sum A_{\mathrm{AC}}}} \tag{12}$$

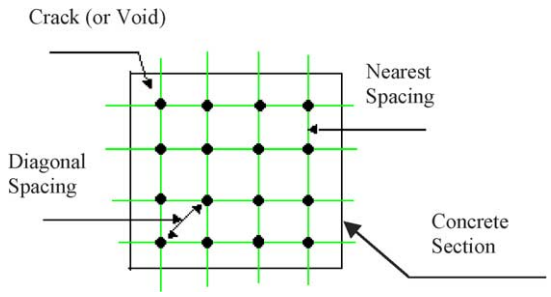

Fig. 5. Schematic presentation of the assumptions used in spacing computations.

3.1.6. Angle of orientation in plane (ω_C)

Direction of concrete cracks can be provided by the angle of orientation. Orientation of concrete cracks can be related to the direction of loading since each different direction of loading may lead to a certain crack orientation. Crack orientation can affect diffusion properties of concrete. Angle of orientation of each individual crack can be determined by measuring angle of crack length inclination on horizontal (X–X) or vertical (Y–Y).

3.1.7. Tortuosity in plane (T_{CP})

Crack Tortuosity is a useful quantitative descriptor of the propagation characteristic of cracks in concrete. Propagation of cracks in concrete depends on the strength of mortar and aggregate. In normal strength concrete, cracking occur in mortar and most of cracks tortuous its path around the aggregate particles and as a result more aggregate particles in concrete leads to more tortuous cracks. Throughout the research study crack tortuosity is expressed as follows:

$$T_{\mathrm{CP}} = \frac{\text{Actual Crack Length}}{\text{Projected Crack Length}} \tag{13}$$

Due to difficulty in measuring the actual crack length, the following expression is generally used:

$$T_{\mathrm{CP}} = \frac{P_{\mathrm{iC}}}{2L_{\mathrm{iC}}} \tag{14}$$

3.1.8. Degree of orientation in plane (Ω_{CP})

While angle of orientation can provide an indication about orientation of each individual crack, degree of orientation provides an indication about the orientation of the overall cracks in the same section. If degree of orientation ($\Omega_p = 1$), this means that the cracks system is completely planar orientated in a certain direction. If degree of orientation ($\Omega_p = 0.0$), this means that the cracks system is completely planar random system [22]. Depending on the value of the Ω_p (between zero and 1) the cracks system can be classified a partially planar oriented system. Assuming cracks as system of lines in the plane, crack degree of orientation in plane can be expressed as follows [22]:

$$\Omega_{\mathrm{CP}} = \frac{[(PL)t \perp -(PL)\mathrm{t}\|]}{[(PL)\mathrm{t} \perp +0.571(PL)\mathrm{t}\|]} \tag{15}$$

3.2. Voids

The area fraction (A_{AV}), perimeter per unit area (P_{AV}), and spacing in plane (λ_{VP}) of voids can be expressed in the same way as for cracks.

3.2.1. Equivalent diameter (d_{LV})

The equivalent circular diameter is the diameter of a fictitious circular that has the same area as the void [23].

The equivalent diameter provides an easy way to estimate the diameter of the void; assuming that the void is spherical in shape. Once the area has been determined, it is often convenient to express it as an equivalent circular diameter and simply calculated from the following expression:

$$d_{\mathrm{LV}} = \sqrt{\frac{4 \times A_{\mathrm{iv}}}{\pi}} \tag{16}$$

3.2.2. Number per unit area (N_{AV})

Number of voids in concrete may be considered to be one of the most important parameters. The importance of the number of voids is owned to its effect on frost resistance and concrete durability and performance. Number of voids can also be used as an indication about the concrete strength, since large number of voids in concrete can lead to low concrete strength. Number of voids in concrete is also helpful in determination void size distribution [24] and some other additional parameters. Number of voids in concrete can be expressed as follows:

$$N_{\mathrm{AV}} = \frac{\sum_{i=1}^{N} N_{\mathrm{iv}}}{\mathrm{Area}} \tag{17}$$

3.2.3. Mean diameter in plane (d_{mvp})

Mean diameter introduces the average diameter of the voids found in a specified concrete section. The mean diameter can be expressed as follows [25]:

$$d_{\mathrm{mvp}} = \sqrt{\frac{4 \times \sum A_{\mathrm{AV}}}{\pi \times N_{\mathrm{AV}}}} \tag{18}$$

3.2.4. Aspect ratio (A_{Sv})

Aspect ratio is a shape index, used to distinguish the change in object elongation. Aspect ratio is close to 1 for spherical voids, and has larger values for elongated ones. Aspect ratio can be used also as a measure for pore size that gives and indication about any pore collapse may occur in the materials due to confining pressure [26]. Aspect ratio is proposed as follows [25]:

$$A_{\mathrm{Sv}} = \frac{L_{\mathrm{iv}}}{W_{\mathrm{vc}}} \tag{19}$$

3.2.5. Form factor (F_{Fv})

Form factor is often used to describe the shape of features. It is usually defined as [27]

$$F_{\mathrm{Fv}} = \frac{4 \times \pi \times A_{\mathrm{iv}}}{(p_{\mathrm{iv}})^2} \tag{20}$$

Form factor reflects the circularity and rough edges of voids; it is maximum at 1.0 for circles and 0.785 for squares.

3.2.6. Compactness (C_{Sv})

Compactness is used to measure the elongation, and is minimum for circles; it is proposed to be expressed as follows:

$$C_{\mathrm{Sv}} = \frac{(P_{\mathrm{iv}})^2}{A_{\mathrm{iv}}} \tag{21}$$

3.2.7. Roundness (R_{Sv})

Roundness is a shape factor similar to form factor, which uses length (longest chord) instead of perimeter; hence it is less sensitive to roughness of boundary and reflects more on elongation. Roundness is expressed as follows [25]:

$$R_{\mathrm{Sv}} = \frac{4 \times A_{\mathrm{iv}}}{\pi \times (L_{\mathrm{iv}})^2} \tag{22}$$

4. Stereological interpretations, in space (3-D) measurement

Stereological relationships use (2-D) measurements performed on two perpendicular sections [(x–y) horizontal and (y–z) vertical]. To quantify the spatial (3-D) structure of microcracks and void systems, the horizontal section was selected to be perpendicular to the predominant loading direction (or, when no loading is involved), perpendicular to the core/specimen length; vertical sections were perpendicular to the horizontal direction. The stereological relationships are introduced below.

4.1. Cracks

4.1.1. Specific surface area (S_{VC})

Specific surface area is the area of cracks per unit volume of concrete. Specific surface area can be considered an indication about the percentage of cracks in the concrete volume and is expressed as follows [28]:

$$S_{\mathrm{VC}} = \frac{4}{3\pi}(2L_{\mathrm{AC1}} + L_{\mathrm{AC2}}) \tag{23}$$

In the case of randomly oriented cracks, the above equation assumes the following form, with (2-D) measurement on one section sufficient to yield the specific surface area of cracks [5,29,30]:

$$S_{\mathrm{VC}} = \frac{4}{\pi} L_{\mathrm{AC}} \tag{24}$$

4.1.2. Volume fraction (V_{VC})

Volume fraction is a parameter that gives an indication about how much concrete specimen contains cracks which can affect most of concrete mechanical properties and it can be expressed as follows:

$$V_{\mathrm{VC}} = \frac{A_{\mathrm{AC1}} + A_{\mathrm{AC2}}}{2} \tag{25}$$

4.1.3. Spacing in space (λ_{CS})

Spacing of cracks in space can considerably affect the thermal properties of concrete such as thermal conductivity and thermal expansion which has a significant effect on concrete shrinkage. Crack spacing in space is considered as the mean free distance and expressed as the following [28]:

$$\lambda_{CS} = \frac{4(1 - V_{VC})}{S_{VC}} \tag{26}$$

4.1.4. Crack width in space (W_{CS})

Cracks are manifested as lines of various thickness on (2-D) cross. The (2-D) crack widths are essentially of minimum crack width measured at non-perpendicular angles to plane of cracks. Fig. 6 shows a schematic presentation of crack widths (W_{CP1} and W_{CP2}) in plane due to cutting by the proposed two perpendicular sections, the actual crack width (W_{CS}) can be obtained as follows:

$$\sin\zeta = \frac{W_{CS}}{W_{CP1}} \tag{27}$$

$$\cos\zeta = \frac{W_{CS}}{W_{CP2}} \tag{28}$$

Since,

$$\sin\zeta^2 + \cos\zeta^2 = 1 \tag{29}$$

From Eqs. (27)–(29), the following equation can be derived:

$$\left(\frac{W_{CS}}{W_{CP1}}\right)^2 + \left(\frac{W_{CS}}{W_{CP2}}\right)^2 = 1 \tag{30}$$

which yields the following expression for (3-D) crack width:

$$W_{CS} = \frac{1}{\sqrt{\frac{1}{w_{CP1}^2} + \frac{1}{w_{CP2}^2}}} \tag{31}$$

4.1.5. Degree of orientation in space (Ω_{CS})

Degree of orientation of cracks in space considers cracks as partially oriented planes in space, and can be expressed as follows [22]:

$$\Omega_{CS} = \frac{[(PL)\mathrm{ts} - (PL)\mathrm{ts}\|]}{[(PL)\mathrm{ts} + (PL)\mathrm{ts}\|]} \tag{32}$$

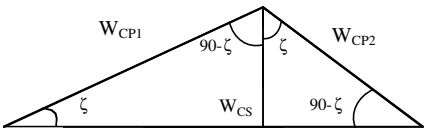

Fig. 6. Schematic presentation of the relationship between projected and actual crack widths.

4.1.6. Tortuosity in space (T_{CS})

Tortuosity of cracks in space is a shape index reflecting on the nature of concrete cracking at failure, and can be expressed as follows:

$$T_{CS} = \frac{T_{CP1} + T_{CP2}}{2} \tag{33}$$

4.2. Voids

4.2.1. Volume fraction (V_{VV})

Voids volume fraction assumes the same values as area fraction, and can be expressed as the average area fraction on the two perpendicular sections.

4.2.2. Number per unit volume (N_{VV})

Number of voids per unit volume can be expressed as follows [22]:

$$N_{VV} = \frac{2 \times m \times N_{AV}}{\pi} \tag{34}$$

where, m is the mean value of the reciprocals of the circle diameters on the test section, which can be expressed as follows [22]:

$$m = \frac{\sum_{d_V=1}^{n}(1/d_{V1}) + (1/d_{V2}) + (1/d_{V3}) + \cdots + (1/d_{Vn})}{n_v} \tag{35}$$

4.2.3. Specific surface area (S_{VV})

Specific surface area of voids is the surface area of voids per unit volume of concrete. Simulating voids as partially oriented linear systems of surfaces in space yields the following expression for specific surface area [22]:

$$S_{VV} = 1.571(PL)\mathrm{ts} \perp + 0.429(PL)\mathrm{ts}\| \tag{36}$$

4.2.4. Mean diameter in space (d_{mvs})

Mean diameter of voids provides a quantitative descriptor of the average size of voids in concrete. Mean diameter of voids can be derived as follows:

$$\text{Volume of sphere } (V) = \frac{4}{3} \times \pi \times \left(\frac{d_v}{2}\right)^3 \tag{37}$$

which yields

$$d_v = \sqrt[3]{\frac{6}{\pi} \times V} \tag{38}$$

In order to obtain the mean diameter of voids in space, volume of voids should be divided by the number of voids in the section of interest yielding the following expression:

$$d_{mvs} = \sqrt[3]{\frac{6 \times V_{VV}}{\pi \times N_{VV}}} \tag{39}$$

4.2.5. Spacing in space (λ_{VS})

Spacing voids in concrete is an important factor to evaluate air-entrained admixtures, since large spacing lead to inefficient influence of air-entrained in concrete and as a the probability of concrete deterioration due to freeze-thaw is increased, while small spacing can adversely affect concrete mechanical properties. Voids spacing in space, can be derived using the same expressions used for cracks.

4.2.6. Specific surface (S_{SV})

Specific surface is the surface area of voids per unit volume of voids and quantifies the irregularity of void surfaces. Void surfaces irregularity is directly proportional to specific surface area value which can is expressed as follows:

$$S_{SV} = \frac{S_{VV}}{V_{VV}} \tag{40}$$

5. Summary and conclusions

An image processing methodology was developed for automated microstructural investigation of concrete, emphasizing microcrack and void systems. A range of (2-D) mathematical formulations was used to quantify planar microstructural features of concrete. Stereological principles were used to derive quantitative information on the (3-D) microstructure of concrete, based on planar measurements. The proposed formulations provide a solid basis for software development towards a quantitative microstructural investigation of concrete microcracks and void systems. The key issue involved in the proposed approach to processing and analysis of concrete microscopic images are summarized below:

1. Thresholding, followed by opening, closing, and hole-fill operations provide the basis to process concrete micrographs with substantial noise. In the case of images with limited noise, thresholding followed by closing, opening, and hole-fill provided a better approach to remove noise and preserve features of interest (microcracks and voids). Opening operations in both causes generally require one to three iterations; closing operations require one to four.
2. New formulations with higher precision were developed to determine crack width in plane and space and crack/void spacing in plane. New specific surface area formulation was adopted to determine crack specific surface area based on the preferred orientation of cracks in concrete.
3. Planar modification of the microcrack system involved formulations of length per unit area, perimeter per unit area, width per unit area, area fraction, degree of orientation, spacing, and tortuosity were produced in systematic system to be programmed in microcrack and void systems quantification software.
4. Planar quantification of the void system involved formulation of equivalent diameter, number per unit area, aspect ratio, form factor, compactness, and roundness were assigned to be the key probes to analyze void systems in concrete and the relationships between these probes and concrete properties were addressed.
5. Planar characteristics of microcracks on two perpendicular sections were used in stereological formulations to quantify microcrack volume fraction, spacing, width, degree of orientation and tortuosity in space. Different spatial formulations for biological applications were adopted to be used for microcrack system analyses.
6. Planar characteristics of voids on two perpendicular sections were used in stereological formulations to quantify the volume fraction, number per unit volume, specific surface area, spacing, and diameter of voids in space.

Acknowledgements

The work reported herein was conducted jointly by DPD, Inc. and Michigan State University under the sponsorship of the US Air Force.

References

[1] Diamond S, Huang J. The ITZ in concrete—a different view based on image analysis and SEM observations. Cem Concr Compos 2001;23:179–88.
[2] Fu Y, Beaudoin JJ. Microcracking as a precursor to delayed ettringite formation in cement systems. Cem Concr Res 1996; 26(10):1493–8.
[3] Young JF. The microstructure of hardened portland cement paste. In: Bazant ZP, Wittmann FH, John, editors. Creep and shrinkage in concrete structures. John Wiley & Sons Ltd.; 1982. p. 3–22.
[4] Lange DA. Image analysis techniques for characterization of pore structure of cement-based materials. Cem Concr Res 1994;24(5): 841–53.
[5] Dequiedt AS, Coster M, Chermant L, Chermant JL. Distances between air-voids in concrete by automatic method. Cem Concr Compos 2001;23:247–54.
[6] Diamond S, Mindess S. SEM investigation of fracture surfaces using stereo pairs: III fracture surfaces of mortars. Cem Concr Res 1994;24(6):1140–1152.
[7] Chiaia B, van Mier JGM, Vervuurt A. Crack growth mechanisms in four different concretes: microscopic observations and fractal analysis. Cem Concr Res 1998;28(1):103–14.
[8] Xuanhui C, Yongqi L. Damage process in hardened cement paste. ACI Mater J 1996;93(4):378–85.
[9] Zhang MH. Microstructure, crack propagation, and mechanical properties of cement pastes containing high volume of fly ashes. Cem Concr Res 1995;25(6):1165–78.
[10] Hakkinen T. The influence of slag content on the microstructure, permeability and mechanical properties of concrete, part 1,

microstructural studies and basic mechanical properties. Cem Concr Res 1993;23(2):407–21.
[11] Jacobsen S, Marchand J, Hornain H. SEM observations of the microstructure of frost deteriorated and self-healed concretes. Cem Concr Res 1995;25(8):1781–90.
[12] Lin W, Lin T, Couche J. Microstructure of fire-damaged concrete. ACI Mater J 1996;93(3):199–205.
[13] Jacbsen S, Gran HC, Sellevold EJ, Bakke JA. High strength concrete-freeze/thaw testing and cracking. Cem Concr Res 1995; 25(8):1775–80.
[14] Shayan A, Quick GW. Microscopic features of cracked and uncracked concrete railways sleepers. ACI Mater J 1992;89(4): 348–61.
[15] St John DA, Polle AW, Sims I. Concrete petrography. John Wiley & Sons Inc; 1998. p. 10–46, 223–46, 283, 286–7 & 289.
[16] Russ JC. Image analysis of the microstructure of materials. In: David BW, Alan RP, Ronald G, editors. Images of materials. Oxford University Press; 1991. p. 338–73.
[17] Konin A, Francois R, Arliguie G. Analysis of progressive damage to reinforced ordinary and high performance concrete in relation to loading. Mater Struct 1998;31:27–35.
[18] Chermant JL, Chermant L, Coster M, Dequiedt AS. Some fields of applications of automatic image analysis in civil engineering. Cem Concr Compos 2001;23:157–69.
[19] Kose S, Guler M, Bahia H, Masad E. Distribution of strains within asphalt binders in HMA using imaging and finite element techniques. In: Transportation research board 79th annual meeting, Washington, DC, 2000. p. 1–21.
[20] Weibel RW. Stereological methods; practical for biological morphometry, vol. 1. Academic Press; 1979. p. 1–3 & 40–5.
[21] Ringot E, Bascoul A. About the analysis of microcracking in concrete. Cem Concr Compos 2001;23:261–6.
[22] Underwood EE. Quantitative stereology. Addison-Wesley Publishing Company; 1970. p. 48–79 & 80–105.
[23] Kuo CY, Freeman RB. Imaging indices for quantification of shape, angularity, and surface texture of aggregate. In: Transportation research board, 79th annual meeting, Washington, DC, 2000. p. 1–22.
[24] Aligizaki KK, Cady PD. Air content and size distribution of air voids in hardened cement pastes using the section-analysis method. Cem Concr Res 1999;29:273–80.
[25] Russ JC. Computer-assisted microscopy, the measurement and analysis of images. Plenum Press; 1990. p. 20–5, 105–15 & 134–48.
[26] Mowar S, Zaman M, Stearns DW, Roegiers JC. Micro-mechanisms of pore collapse in limestone. J Petrol Sci Eng 1996;15: 221–35.
[27] Russ JC. Practical stereology. New York: Plenum Press; 1986. p. 103–20.
[28] Weibel RW. Stereological methods; practical for biological morphometry, vol. 2. Academic Press; 1979. p. 261–3 & 299–305.
[29] Petrov I, Schlegel E. Application of automatic image analysis for the investigation of autoclaved aerated concrete structure. Cem Concr Res 1994;24(5):830–40.
[30] Mobasher B, Stang H, Shah SP. Microcracking in fiber reinforced concrete. Cem Concr Res 1990;20:665–76.

Parviz Soroushian, Fellow of ACI, is a Professor of Civil and Environmental Engineering at Michigan State University. His specialty is in materials engineering; he has authored more than 100 technical publications and holds 15 patents in this field. He is past Chair of ACI Committee 549.

Mohamed Elzafraney received his BS and MS degrees from Alexandria University, Egypt, and is currently a PhD candidate in Civil Engineering Department, Michigan State University. His research interests include concrete microstructure and concrete durability.